ISSN 0031-918X, Physics of Metals and Metallography, 2022, Vol. 123, No. 10, pp. 1024–1030. © Pleiades Publishing, Ltd., 2022.
Russian Text © The Author(s), 2022, published in Fizika Metallov i Metallovedenie, 2022, Vol. 123, No. 10, pp. 1092–1098.

STRENGTH AND PLASTICITY

Surface Hardening of High-Nitrogen Austenitic Steel by Severe Deformation–Heat Treatment

N. A. Narkevich[a], *, M. N. Volochaev[b], I. A. Shulepov[a], and Yu. F. Gomorova[a]

[a] *Institute of Strength Physics and Materials Science, Siberian Branch, Russian Academy of Sciences, Tomsk, 634055 Russia*
[b] *Kirensky Institute of Physics, Siberian Branch, Russian Academy of Sciences, Krasnoyarsk, 660036 Russia*
**e-mail: natnark@list.ru*

Received April 14, 2022; revised July 12, 2022; accepted July 15, 2022

Abstract—The structure and mechanical properties of austenitic high-nitrogen steel (16.5 Cr, 18.8 Mn, 0.07 C, 0.53 N, 0.52 wt % Si, Fe for balance) have been investigated after severe deformation–heat treatment, which has involved shock surface forging at the ultrasonic frequency (USF) and electron-beam heat treatment (EBT). A subgrain structure hardened by CrN nanoparticles has been shown to form in the surface layer as a result of deformation–heat treatment. No discontinuous decomposition of austenite with the formation of Cr_2N nitrides takes place. This structure modification in the surface layer enhances the strength properties of the steel, namely, $\sigma_{0.2}$ increases to 712 MPa and σ_u to 923 MPa at a plasticity of 25%. The yield strength increases by 50% compared to the state after quenching.

Keywords: high-nitrogen steel, austenite, ultrasonic forging, electron beam treatment, aging, CrN, strength, plasticity

DOI: 10.1134/S0031918X22601007

INTRODUCTION

Austenitic stainless Cr–Mn–N steels with low stacking fault energy (SFE) are best hardened by cold plastic deformation. Therefore, a great interest in the study of deformation mechanisms, mechanical properties, and structural transformations that occur in these steels during different deformation treatments is natural [1–12]. The deformation-induced hardening is more effective than precipitation hardening [12–14]. The aging of high-nitrogen steels after quenching, similarly to cold-deformed steels, involves the decomposition of austenite and formation of CrN and Cr_2N chromium nitrides. The hardening of steels depends on the properties of nitrides, their morphological features, volume fraction, size, distribution in austenite, and their relation with the matrix. Aging has no significant effect on the strength properties of steels [13]. However, as shown in [1], the additive contribution of deformation-induced and precipitation hardening during warm rolling permit us increasing the strength properties, while maintaining satisfactory plasticity.

CrN and Cr_2N nitrides have FCC and HCP lattices, respectively. The microhardness of CrN is less than that of Cr_2N, namely 10.8 GPa and 15.7 GPa according to some data [15, 16] and 18.0 GPa and 29.5 GPa according to other data [17], respectively, given close values of elastic moduli (319.8, 310 GPa) [15, 16]. This results in a higher brittleness of Cr_2N; therefore, aging with the formation of CrN is preferable to the precipitation of Cr_2N nitrides. The morphology of the aging-induced nitrides is also different.

Discontinuous decomposition of austenite produces Cr_2N plates mainly at grain boundaries [13, 18]. They form due to the diffusion of alloying elements along grain boundaries [14]. Austenite decomposition and the formation of Cr_2N nitrides in a defective structure containing deformation twins and slip bands can occur via a continuous mechanism [14].

CrN particles have a shape close to globular and they form only by the continuous mechanism. CrN nitride was noted to be unstable and transformed into Cr_2N nitride when the aging time increases [19].

The structure and mechanical properties can be improved by controlling precipitation hardening mechanisms and the type of nitrides that are formed. Solving this task using traditional heating or thermomechanical processing techniques is difficult. First, the technological difficulties of cold or warm rolling, especially for large-sized billets, cause problems. Second, the low heating rate during warm rolling or furnace heating after cold rolling are unable to prevent the CrN $\rightarrow$ Cr_2N nitride transformation, which reduces both the strength and ductility properties.

We believe that a hardening treatment that combines severe cold deformation of only the surface layer of high-nitrogen steel and subsequent high-rate heat treatment is more promising. This work focuses on the

Table 1. The chemical composition of the steel

Composition	Cr	Mn	Si	Ni	C	N	P	S	Fe
wt %	16.50	18.81	0.52	0.24	0.07	0.53	0.01	0.001	Balance

mechanical properties and structure formed during deformation–heat treatment, due to which hardening is achieved by the additive effect of deformation and precipitation hardening mechanisms.

EXPERIMENTAL

The chemical composition of the Cr–Mn–N steel is shown in Table 1. The steel was melted under equilibrium conditions in a 50 kg laboratory induction furnace with chromium–magnesite lining. After water quenching from 1100°C, the steel had a single-phase austenitic structure with an average grain size of 40 μm and contained no insoluble nitride phases. The surface of the steel plate with a thickness of 10 mm, a width of 20 mm, and a length of 100 mm was ground and polished with diamond pastes beforehand. This surface was then severely deformed by forging with strikers at ultrasonic frequency, i.e., ultrasonic forging (USF). USF of the surface was carried out using a UZG 06/27 ultrasonic generator (output power 550 W, generator frequency 25 kHz, transducer amplitude 15 μm) at room temperature in air. Three axially moving strikers (parts of working tool), working asynchronously, were pressed to the machined surface at a load of 70 N. The load and vertical movements of the strikers were provided by a spring, which was a part of the working tool. The speed of the machined surface relative to the working tool was 20 mm/s. A sample was heated to no more than 50°C during deformation. The USF was described in detail in [20].

After the deformation treatment, the steel plate surface was subjected to electron-beam treatment (EBT) on an ELU-5 unit modernized at the Institute of Strength Physics and Materials Science, Siberian Branch, Russian Academy of Sciences, at a residual pressure of 0.1 Pa [21]. The electron beam was swept in a line 20-mm long and 0.5-mm wide perpendicular to the direction of the movement of the plate. The EBT was performed by moving a high-nitrogen steel plate relative to the electron beam at a speed of 15 mm/s. The EBT parameters were as follows: the electron beam sweep frequency was 200 Hz, the electron beam current was $I = 0.02$ A, and the maximum electron energy was 27 keV. The time of maximum heating of each point on the surface was about 3.3×10^{-2} s. After the treatment, the steel was cooled in a vacuum chamber.

The results of preliminary trial experiments were taken into account to choose an EBT mode. EBT at a higher power density of the electron beam melted the surface and resulted in the formation of a defect-free structure with an average grain size of the micron scale (1–2 μm), i.e., the structure formed by USF was neutralized. A decrease in the speed of the processed plate relative to the electron beam had a similar effect on the surface structure. The treatment at a lower electron beam power density decreased the thickness of the layer with the modified structure. This limited the ability to experimentally investigate the effect of deformation–heat treatment on the structure and mechanical properties (in addition to nanohardness). In addition, the formation of a layer that is too thin reduces the potential of this treatment for industrial use to harden the surface of high-nitrogen steels.

Samples for mechanical tests were cut from the plate by electrosparking so that only one surface was subjected to deformation–heat treatment. The gage part of a sample was 15 mm in length and 2.5 × 1 mm in cross section. The properties were determined by testing three samples per point. Tensile mechanical tests were performed using an INSTRON 5582 (USA) tester at room temperature and a strain rate of 1.87×10^{-4} s^{-1} until failure. For comparison, samples after quenching and ultrasonic treatment were tested under similar conditions.

The structure of the steel surface layer was examined by electron backscattered diffraction (EBSD) on a Quanta 200 3D apparatus. The same apparatus was used to study fractograms of fractures. Foils for electron microscopic examinations were cut in the "cross-section" geometry using a Hitachi FB-2100 focused ion beam system (Japan). The structure was then examined using an HT-7700 transmission electron microscope (TEM; Hitachi, Japan) at an accelerating voltage of 120 kV.

RESULTS AND DISCUSSION

Structure Examination

The structure of the surface layer after USF is highly dispersed (Fig. 1a). Nanoscale fragments of austenite are misoriented relative to each other and form rings in the electron diffraction pattern (Fig. 1b). The structure refinement during USF is accompanied by strain aging, during which CrN nitride with a FCC lattice forms. Strain aging is one of the factors that affect the reduction of the austenite lattice parameter described in [19]. USF-induced severe plastic deformation was shown [22] to result in the formation of another nitride, Fe_2N, which, like CrN, has a larger lattice parameter compared to that of the austenite lattice. An increase in local static atomic displacements from the equilibrium positions in the FCC lattice assists in strain aging. After USF in the directions ⟨100⟩

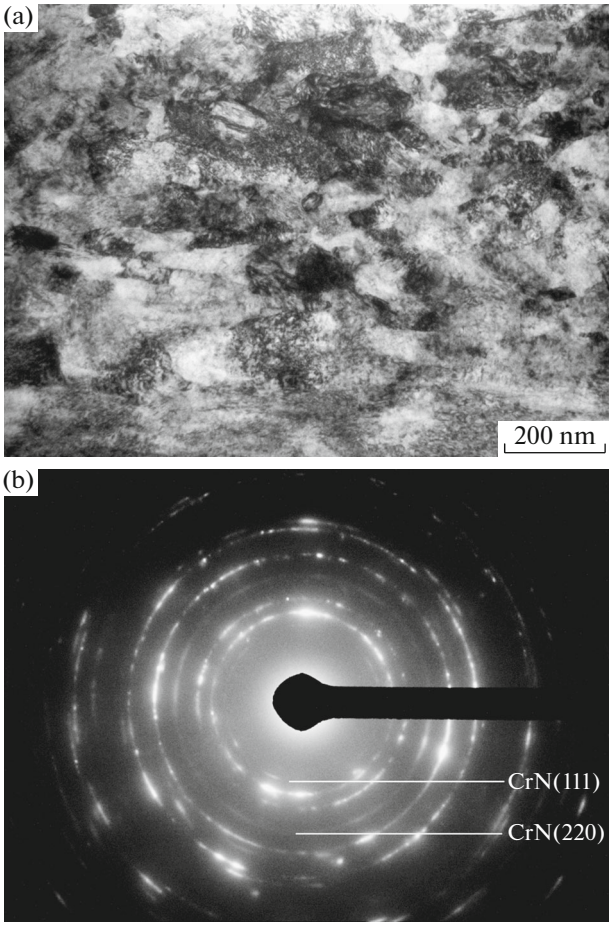

Fig. 1. The structure of Cr–Mn–N steel after USF treatment: (a) bright-field image and (b) electron diffraction pattern.

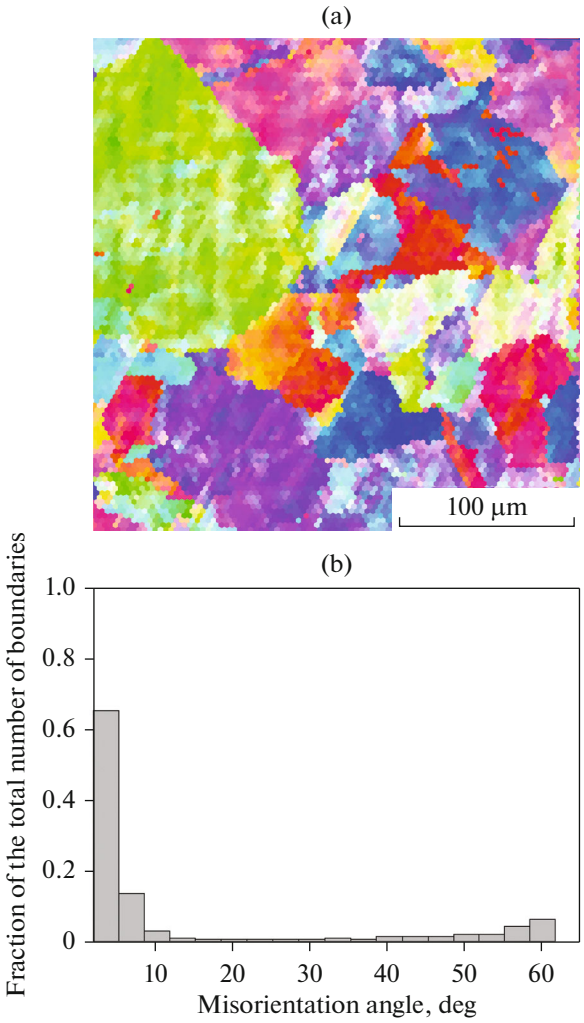

Fig. 2. (a) An EBSD map of the Cr–Mn–N steel after deformation–heat treatment (USF + EBT) and (b) misorientation angle distribution of boundaries.

and ⟨111⟩, the static displacements reach 4.6×10^{-3} and 2.7×10^{-3} nm, respectively [23]. These displacements form regions of both local tension and local compression. The stress state [23], high concentration, and mobility of strain-induced vacancies [24] in combination with local strain heating promote an increase in the diffusion mobility of nitrogen atoms and formation of chemical bonds with Cr and Fe atoms. Phases with a higher specific lattice volume than that of austenite (V_{CrN} = 70.855 Å^3, V_{Fe_2N} = 135.13 Å^3, V_γ = 47.7 Å^3) form in the regions of local tension. The relaxation process in the form of strain aging, according to [25], continues up to low temperatures. The locally high deformation heating is shown in [11, 22]. These works show that severe plastic deformation does not result in the formation of ε martensite with HCP lattice in the surface layer due to direct and reverse $\gamma \rightarrow \varepsilon \rightarrow \gamma$ transformations, while it forms under other deformation conditions, such as tension at room temperature [6].

After deformation–heat treatment, the austenite nanostructure transforms mainly into a subgrain structure with predominantly low-angle boundaries having misorientations of less than 5° (Fig. 2). Static atomic displacements from equilibrium positions in the FCC lattice were observed to decrease to 4.4×10^{-3} and 2.0×10^{-3} nm in the ⟨100⟩ and ⟨111⟩ directions, respectively, compared to the post-USF state [23]. A more equilibrium structure formation is associated with a decrease in its defectiveness, as well as with the decomposition of supersaturated solid solution. Dispersion hardening in this structure occurs by a continuous mechanism with the formation of CrN nitrides with a FCC lattice, and without the formation of Cr_2N (Fig. 3). The size of CrN particle varies from 1 to 10 nm.

It is difficult to distinguish CrN particles from nitrides with FCC lattices and close interplanar distances when there are other nitride-forming elements besides chromium in the composition of steels [1, 26, 27]. For comparison, CrN, VN, and Mo_2N have FCC lattices and

close interplanar distances (2.395, 2.382, 2.406 Å for plane (111), respectively, 2.074, 2.063, 2.084 Å for plane (200), etc.). The probability of the formation of a particular nitride during aging of complex alloy steels with several nitride forming elements can be estimated by the energy of their formation and taking into account the concentration of nitride-forming elements in the steel. The most reliable results of research on the factors that determine the formation of CrN particles, but not Cr_2N in high-nitrogen steels are found in [19, 22, 28]. For example, nitrides CrN formed in steel containing 17% Cr, 6.5% Ni, 1.3% Mn, and 0.15% N [19] after quenching, cold rolling by 63%, and subsequent aging with heating at a rate of 200 K/s to a temperature of 600°C and short exposure time from 1 to 10 sec and the same accelerated cooling at a rate of 200 K/s. Our studies [22], as well as the present work, show that CrN nitrides can be formed by severe plastic deformation. Short-term severe heat treatment with an electron beam after USF increases the volume fraction of cubic chromium nitrides. According to [28], CrN particles that are isomorphic to austenite form in steel containing 18% Cr, 2% Ni, and 0.9% N, without preliminary deformation, but upon quenching and low-temperature aging at 350°C for 2 h. The authors do not discuss the effect of steel melting technique and nitrogen alloying on the aging mechanism. However, the high nitrogen content in the steel indicates that the conditions of steel production were not equilibrium, i.e., the nitrogen pressure was higher than atmospheric pressure, as in [26, 27]. We believe that this factor is key in activating aging by a continuous mechanism with the formation of CrN, since nitrogen atoms in a concentration exceeding the equilibrium one, except in nitrides, cannot exist. CrN particles seem to already exist in the volume of austenitic grains after quenching.

In summary, preliminary formation of a defect dislocation structure that creates conditions for the heterogeneous nucleation of CrN particles is a necessary condition for the precipitation hardening of high-nitrogen steels with equilibrium nitrogen content. Another treatment parameter is the thermal condition. High-temperature, but short-term heating and high-rate cooling prevent the formation of Cr_2N nitrides and the $CrN \rightarrow Cr_2N$ transformation.

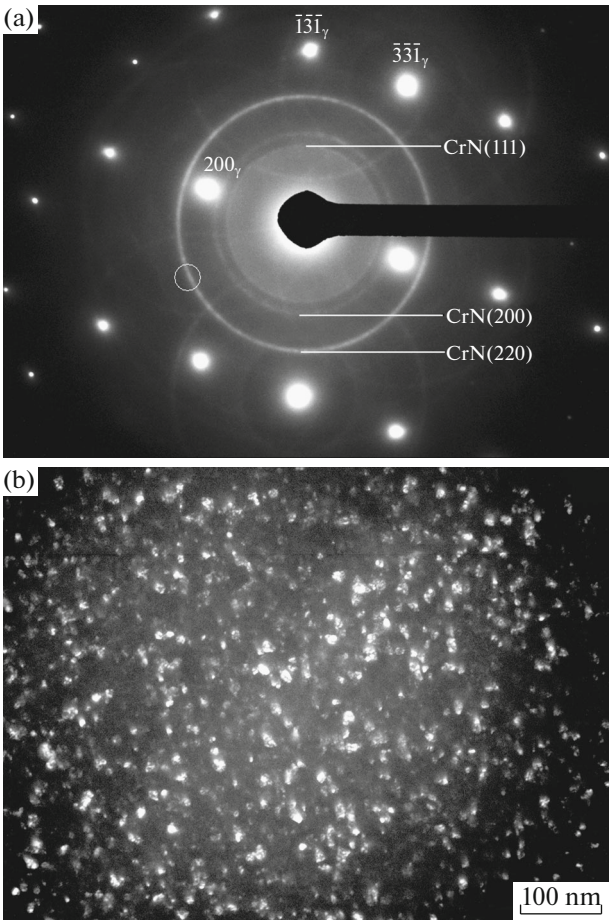

Fig. 3. The structure of the Cr–Mn–N steel after deformation–heat treatment (USF + EBT): (a) electron diffraction pattern with zone axis $[01\bar{3}]_\gamma$ and (b) dark-field image taken in the $(220)_{CrN}$ reflection indicated by the corresponding ring.

Mechanical Properties

Figure 4a shows σ–ε curves for the steel that was tested in different structural states. The yield strength of the steel increases and the ultimate tensile strength remains at the same level after the first stage of deformation–heat treatment (surface USF). A similar result was achieved when tested at negative temperatures down to –80°C [22]. An increase in the resistance to deformation at the initial stage results in a decrease in the relative elongation (Table 2). We

Table 2. The mechanical properties of Cr–Mn–N steel

Treatment	Yield strength $\sigma_{0.2}$, MPa	Ultimate tensile strength σ_u, MPa	Relative elonfation ε, %
Quenching	480	855	65
Quenching + USF	600	890	42
Quenching + USF + EBT	712	923	25

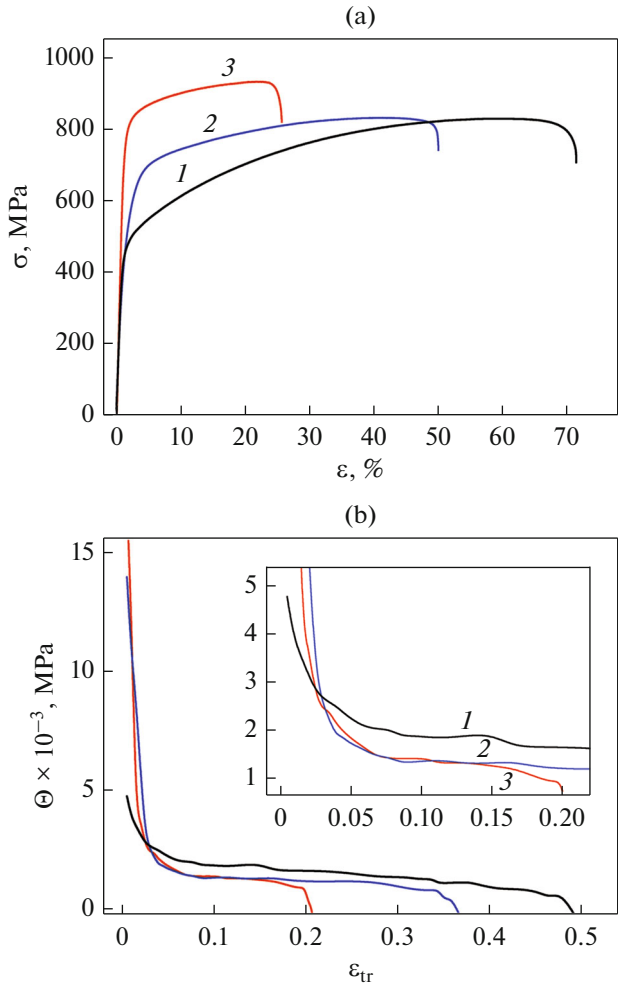

Fig. 4. (a) The curves σ–ε and (b) strain rate hardening rate of Cr–Mn–N steel during tensile tests after (*1*) quenching from 1100°C, (*2*) after quenching and USF, and (*3*) after deformation–heat treatment (USF + EBT).

showed [22] that a sample after USF started to fracture from a nanostructured surface layer during mechanical tests. Its thickness did not exceed 150 μm. Further, the deformation develops outside this layer, but deformation is localized under microcrack tops, which reduces plasticity.

The second stage of the deformation–heat treatment results in an additional increase in both the yield strength and tensile strength (Fig. 4a, Table 2). A plasticity decrease up to 25% after deformation-heat treatment can be explained by the fact that the heat effect upon EBT extends not only to the surface layer, but also to a greater depth, exceeding 150 μm. Aging in this case takes place across the entire cross-section of the sample. This can explain both the decrease in plasticity and the increase in the tensile strength (Fig. 4a).

The strain rate hardening of the samples with modified surface layers at the initial stage of deformation at $\varepsilon < 0.03$ is higher than that of the quenched samples (Fig. 4b). However, the deformation hardening in the samples hardened by USF and USF + EBT proceeds less intensively than that in the quenched sample with increasing strain rate $\varepsilon > 0.03$ and up to fracture. This is also shown by the safety factor of steel $K = \sigma_u/\sigma_{0.2}$ after quenching, after USF and after USF + EBT, equal to 1.83, 1.49, and 1.30, respectively.

Fracture Surface

Comparison of fracture fractograms (Fig. 5) shows that the steel after all deformation-heat treatment stages fractures in a ductile manner. One can note no necking in the hardened layer after USF and deformation-heat treatment, unlike that in the sample after quenching. This result agrees with the appearance of the σ–ε curves (Fig. 4), where along with a decrease in the total strain, a decrease in the localized strain stage is observed during the transition from one stage of the deformation–heat treatment to another. The sizes of dimples in a surface layer fracture after USF and deformation–heat treatment do not differ significantly. The shape of the dimples in both cases is predominantly equiaxed (Fig. 5c), which indicates tearing fracturing.

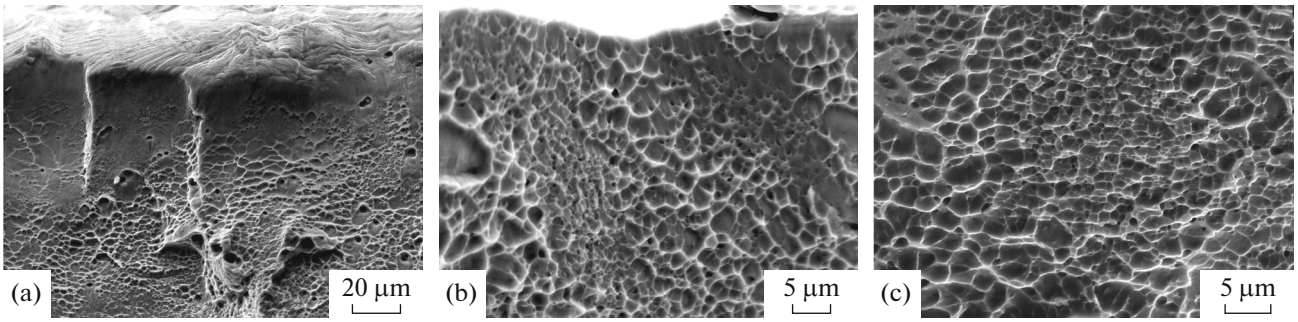

Fig. 5. Fractograms of the Cr–Mn–N steel subjected to tensile tests after (a) quenching from 1100°C, (b) USF, and (c) deformation–heat treatment (USF + EBT).

CONCLUSIONS

(1) Deformation–heat treatment of Cr–Mn–N steel in the form of severe plastic deformation by shock treatment at ultrasonic frequency and subsequent high-rate heating by scanning electron beam caused the formation of a subgrain austenite structure in the surface layer. This structure, which was hardened by CrN nanoparticles with the FCC lattice, was characterized mainly by low-angle misorientations up to 5°. Austenite decomposition occurs by a continuous mechanism with heterogeneous precipitation of CrN particles.

(2) The deformation–heat treatment improves the strength properties of the steel, namely, $\sigma_{0.2}$ increases to 712 MPa and σ_u increases to 923 MPa at a plasticity of 25%.

(3) The surface layer of the investigated steel, which contains CrN nitrides, fractures in a tearing and ductile manner after a two-stage deformation-heat treatment, inheriting the shape and size of dimples from the previous deformation treatment.

ACKNOWLEDGMENTS

Structural examination was carried out using the equipment of the Krasnoyarsk Regional Center of Collective Use, Siberian Branch, Russian Academy of Sciences. EBSD analysis was performed on the equipment of the Tomsk Materials Science Center for collective use at Tomsk State University.

FUNDING

This work was performed within the state assignment of the Institute of Strength Physics and Materials Science, Siberian Branch, Russian Academy of Sciences (theme no. FWRW-2021-0009).

CONFLICT OF INTEREST

The authors declare that they have no conflicts of interest.

REFERENCES

1. V. V. Sagaradze and A. I. Uvarov, *Strengthening and Properties of Austenitic Alloys* (RIO UrO RAN, Yekaterinburg, 2013) [in Russian].
2. Yu. P. Solntsev, *Cold-Resistant Steels and Alloys* (Khimizdat, St. Petersburg, 2005) [in Russian].
3. S. C. Sun, J. W. Mu, Z. H. Jiang, C. T. Ji, J. S. Lian, and Q. Jiang, "Effect of cold rolling on tensile properties and microstructure of high nitrogen alloyed austenitic steel," Mater. Sci. Technol. **30** (2), 146–151 (2014).
4. A. D. Korotaev, A. N. Tyumentsev, and I. Yu. Litovchenko, "Defect substructure and stress fields in the zones of deformation localization in high-strength metallic alloys," Phys. Met. Metallogr. **90** (Suppl. 1), 36–47 (2000).
5. M. Milititsky, D. K. Matlock, A. Regully, N. Dewispelaere, J. Penning, and H. Hanninen, "Impact toughness properties of nickel-free austenic stainless steels," Mater. Sci. Eng., A **496** (1–2), 189–199 (2008).
6. N. A. Narkevich and N. S. Surikova, "Deformation behavior and structure evolution of stainless Cr–Mn–N steel during low temperature tension," Phys. Met. Metallogr. **121** (12), 1175–1181 (2020).
7. N. Narkevich, Ye. Deryugin, and Yu. Mironov, "Effect of the $\gamma \rightarrow \varepsilon$ phase transition on transformation-induced plasticity (TRIP) of nickel-free high nitrogen steel at low temperatures," Metals **11** (5), 710 (2021).
8. V. A. Shabashov, K. A. Lyashkov, N. V. Kataeva, L. G. Korshunov, V. V. Sagaradze, and A. E. Zamatovskii, "Inversion of nitrogen redistribution in austenitic steel by severe plastic deformation," Phys. Met. Metallogr. **122** (7), 657–664 (2021).
9. P. K. Rai, V. Pandey, K. Chattopadhyay, L. K. Singhal, and V. Singh, "Effect of ultrasonic shot peening on microstructure and mechanical properties of high-nitrogen austenitic stainless steel," J. Mater. Eng. Perform. **23** (11), 4055–4064 (2014).
10. L. G. Korshunov, V. V. Sagaradze, N. L. Chernenko, N. L. Pecherkina, G. Yu. Kalinin, S. Yu. Mushnikova, and O. A. Khar'kov, "Structure and tribological properties of nitrogen-containing austenitic steels," Vopr. Materialovedeniya **71** (3), 136–145 (2012).
11. V. V. Sagaradze, N. V. Kataeva, I. G. Kabanova, S. V. Afanasev, and A. V. Pavlenko, "Effect of the temperature of shock-wave loading on structure and phase transformations in nitrogen-containing austenitic Cr–Mn–Ni steel," Phys. Met. Metallogr. **121** (7), 683–688 (2020).
12. L. B. Zuev, N. A. Dubovik, and V. E. Pak, "Nature of hardening of high-nitrogen steels based on iron-chromium-manganese austenite," Steel Transl. **27** (10), 71–75 (1997).
13. J. W. Simmons, "Overview: high-nitrogen alloying of stainless steels," Mater. Sci. Eng., A **207**, 159–169 (1996).
14. B. Kartik, R. Veerababu, M. Sundararaman, and D. V. V. Satyanarayana, "Effect of temperature ageing on microstructure and mechanical properties of a nickel-free high nitrogen austenitic stainless steel," Mater. Sci. Eng., A **642**, 288–296 (2015).
15. M. Pakala and R. Y. Lin, "Reactive sputter deposition of chromium nitride coatings," Surf. Coat. Technol. **81** (2–3), 233–239 (1996).
16. J.-N. Tu, J.-G. Duh, and S.-Yu. Tsai, "Morphology, mechanical properties, and oxidation behavior of reactively sputtered Cr–N films," Surf. Coat. Technol. **133–134** (2–3), 181–185 (2000).
17. A. Tricoteau, P. Y. Jouan, J. D. Guerin, J. Martinez, and A. Djouadi, "Fretting wear properties of CrN and Cr_2N coatings," Surf. Coat. Technol. **174–175** (2–3), 440–443 (2003).
18. I. F. Machado and A. F. Padilha, "Aging behavior of 25Cr–17Mn high nitrogen duplex stainless steel," ISIJ Int. **40** (7), 719–724 (2000).
19. S. Rajasekhara, L. P. Karjalainen, A. Kyröläinen, and P. J. Ferreira, "Microstructure evolution in nano/sub-

micron grained AISI 301LN stainless steel," Mater. Sci. Eng., A **527**, 1986–1996 (2010).

20. N. A. Narkevich, A. I. Tolmachev, I. V. Vlasov, and N. S. Surikova, "Structure and mechanical properties of nitrogen austenitic steel after ultrasonic forging," Phys. Met. Metallogr. **117** (3), 288–294 (2016).
21. V. E. Panin, S. I. Beljuk, V. G. Durakov, G. A. Pribytkov, and N. G. Rempe, "Electron beam vacuum surfacing: Equipment, technology and properties of coatings," Weld. Int. **14** (7), 580–584 (2000).
22. N. A. Narkevich, E. E. Deryugin, and I. V. Vlasov, "Effect of ultrasonic forging strain processing on the surface layer microstructure and temperature-dependent mechanical properties of high nitrogen austenitic steel," Mater. Sci. Eng., A **834**, 142590 (2022).
23. N. Narkevich, N. Surikova, I. Vlasov, V. Narkevich, Ye. Deryugin, and O. Perevalova, "Effect of electron beam treatment on the elemental composition and static displacements of atoms in the nearsurface layer of Cr–Mn–N austenitic steel," AIP Conf. Proc. **2167**, 020238 (2019).
24. V. A. Shabashov, V. V. Sagaradze, and A. V. Makarov, "Structure modification of high-nitrogen and high-carbon austenitic steels by megadeformation," Phys. Met. Metallogr. **119** (11), 1087–1092 (2018).
25. V. A. Shabashov, A. V. Makarov, K. A. Kozlov, V. V. Sagaradze, A. E. Zamatovskii, E. G. Volkova, and S. N. Luchko, "Deformation-induced dissolution and precipitation of nitrides in austenite and ferrite of a high-nitrogen stainless steel," Phys. Met. Metallogr. **119** (2), 180–190 (2018).
26. V. V. Berezovskaya and E. A. Merkushkin, "Features of decomposition of a supersaturated γ-solid solution in Cr–Mn high-nitrogen steels on heating," Vestnik Tambovskogo Universiteta. Ser. Estestvennye i Tekhnicheskie Nauki **21** (3), 897–900 (2016).
27. B. B. Berezovskaya, Yu. A. Raskovalova, E. A. Merkushkin, and R. Z. Valiev, "Twip-effect in nickel-free high-nitrogen austenitic Cr–Mn steels," Met. Sci. Heat Treat. **57**, 656–662 (2016).
28. V. V. Berezovskaya, I. V. Golyakov, O. A. Bannykh, and V. M. Blinov, "Effect of cold plastic deformation on the structure and corrosion resistance of austenitic aging 0Kh18N2A alloy," Metally **2006** (5), 390–393 (2006).

Translated by T. Gapontseva